Available online at www.sciencedirect.com
SCIENCE DIRECT®
Journal of Solid State Chemistry 177 (2004) 4443–4450
JOURNAL OF SOLID STATE CHEMISTRY
www.elsevier.com/locate/jssc

XRD and Mössbauer studies of crystallographic and magnetic transformations in synthesized Zn-substituted Cu–Ga–Fe compound

S.S. Ata-Allah*

Reactor and Neutron Physics Department, Nuclear Research Center, Atomic Energy Authority, P.O. Box Enshase, Cairo 13759, Egypt

Received 9 February 2004; received in revised form 16 July 2004; accepted 15 September 2004

Abstract

System of samples in the form of $Cu_{1-x}Zn_xFe_{2-y}Ga_yO_4$ with ($0.0 \leqslant x \leqslant 1.0$, $y = 0.0$ and 1.0) is synthesized. X-ray diffraction study confirms the presence of a single-phase structure, where tetragonal unit cell is obtained for samples $CuFe_2O_4$ and $CuGaFeO_4$ with $c/a > 1$. At compositional parameter $x \geqslant 0.25$, tetragonal-to-cubic transformation occurs. The determined lattice parameter a for the cubic samples is found to decrease with increasing Zn content x. ^{57}Fe Mössbauer measurements at 293, 77 and 12 K show characteristic spectra of paramagnetic, magnetic, and electronic types for the different compositions. Cation distribution obtained from the spectral analysis at 12 K revealed transformation from the ferrimagnetic inverse spinel of $CuFe_2O_4$ to the antiferromagnetic normal spinel of $ZnFe_2O_4$. Hyperfine parameters are found to be strongly dependent on temperature and concentration parameter x. Low-temperature measurements are carried out using installed and well-calibrated closed-cycle variable temperature cryostat Model REF-399-D22. Low vibration is obtained through bellows, spacer, and exchange gas isolation and a difference of $0.018\,mm\,s^{-1}$ between the FWHM of a pure iron foil at room temperature and 12 K is achieved.

Keywords: Tetragonal-to-cubic transformation; Magnetic transformation; Closed-cycle variable temperature cryostat for Mössbauer

1. Introduction

Spinels with AB_2O_4 formula are ternary oxides that have important technological applications: including use as magnetic materials [1], superhard materials [2], high-temperature ceramics [3] and high-pressure sensors [4]. In particular, the phase transformations and Jahn–Teller (JT) distortion in the tetragonal spinels have attracted considerable attention in recent studies [5–8]. JT distortions in the spinel structure have been widely studied from the viewpoint of the arrangement in a lattice of the orbital directions of certain anisotropic ions. In the ideal cubic AB_2O_4 spinel structure the oxygen ions form a cubic close packed lattice with the A and B cations occupying, respectively, 1/8 of the tetrahedrally and 1/2 of the octahedrally coordinated interstices. The large tetragonal distortion, which occurs in a number of spinels such as $ZnMn_2O_4$, $CuFe_2O_4$ and $CuCr_2O_4$, arises because of JT-type distortion in the immediate environment of ions with d^4, d^9 in a high spin state [9–11]. The cooperative JT effect has also been observed, because of higher concentrations of JT ions in the octahedral site, which are either isolated from each other or connected in one, two, or three dimensions via common corners, edges, or laces [12]. Copper ferrite, which is tetragonal at room temperature due to a cooperative JT distortion that is driven by the octahedral-site Cu^{2+} ($3d^9$) ions, has led to a number of experimental and theoretical investigations of this phenomenon [13].

Diamagnetic substitutions in simple and mixed ferrites have received a great deal over the past years [14,15]. The presence of non-magnetic ions in spinel ferrites is found to alter their magnetic and electric properties. Such isomorphous substitutions in iron

*Corresponding author. Fax: +20 2 462 0778.
E-mail address: ssatallah@hotmail.com (S.S. Ata-Allah).

0022-4596/$ - see front matter © 2004 Elsevier Inc. All rights reserved.
doi:10.1016/j.jssc.2004.09.021

oxides are particularly apparent in their Mössbauer spectra, since these will drastically reduce magnetic interactions, resulting in lower magnetic ordering temperature and decreased magnetic field supertransfer (i.e., lower hyperfine fields) [16–19].

The present work reports the preparation procedures and the results of X-ray diffraction (XRD) and Mössbauer studies of Zn^{2+}-substituted Cu-gallate spinel ferrites $Cu_{1-x}Zn_xFe_{2-y}Ga_yO_4$ with ($0.0 \leqslant x \leqslant 1.0$, $y = 0.0$ and 1.0) aiming to shed more lights on crystallographic structure and the microscopic picture of the magnetic ordering in these diluted ferrimagnets. In addition, installation and optimization of Mössbauer closed-cycle cryogenic variable temperature workstation is done for the low-temperature measurements.

2. Experimental details

2.1. Sample preparation

Polycrystalline samples of $CuFe_2O_4$, $ZnFe_2O_4$ and $Cu_{1-x}Zn_xFeGaO_4$ with ($0.0 \leqslant x \leqslant 1.0$) are synthesized through solid-state reactions using Fe_2O_3, ZnO, CuO, and Ga_2O_3 (with purity $\geqslant 99.99\%$) as starting materials. The mixture of the oxide powders is prefired at 950–1100 °C depending on the CuO content, for 72 h. The product is reground and fired again at the same conditions to improve homogeneity. The final powders are pressed into pellets and sintered at 1000–1200 °C for 8 h, then slowly cooled to room temperature. XRD measurements are obtained using Co$K\alpha$ radiation and their analysis showed that the products are crystallized in a single-phase structure.

2.2. Mössbauer experiment and setup for 12 K measurements

Austin Science Mössbauer Spectrometer with constant acceleration laser-interferometer-controlled drive and data acquisition system is used in a standard transmission setup with a Personal Computer Analyzer (PCA II-card with 1024 channels). The radioactive source is ^{57}Co imbedded in Rh matrix with initial activity of 50 mCi. Metallic iron spectrum is used for the calibration of hyperfine magnetic fields. The absorber thickness is approximately 10 mg cm^{-2} of natural iron. Measurements at 77 K are carried out using Oxford liquid-nitrogen cryostat Model (DN1726) with temperature controller Model ITC^{502}. For the low-temperature measurements (12 K), the closed-cycle variable temperature cryostat for Mössbauer (Model REF-399-D22) is installed, optimized and utilized. The temperature achieves 12 K, in a cooling-down time of 2.5 h from room temperature and 11.5 K for continuous use. Low vibration is obtained through bellows, spacer, and exchange gas isolation. Fig. 1 shows the Mössbauer effect (ME) spectra of a pure Fe foil with thickness $t = 35\,\mu$m at room temperature and 12 K, where the fitting of the spectral lines yields values of 0.292 and 0.31 mm s^{-1} for the FWHM at room temperature and 12 K, respectively. Therefore, a difference of 0.018 mm s^{-1} between the FWHM of the two spectra is achieved. Temperature is maintained constant to ± 0.01 K during the measurements using Model 22 Cryogenic Temperature Controller and turbo molecular pump Model (BH2-60). The ME spectra are analyzed with a computer program [18], where the areas of both tetrahedral and octahedral subspectra of the Fe^{3+} are used for determination of cation distribution.

3. Results and discussions

Fig. 2 shows the XRD patterns of the prepared samples $CuFe_2O_4$, $ZnFe_2O_4$ and $Cu_{1-x}Zn_xGaFeO_4$ with ($0.0 \leqslant x \leqslant 1.0$). The diffraction peaks are fitted by modified Gaussian functions, and the lattice parameters are obtained by fitting the diffracted peaks using standard least squares methods. The result of indexing XRD patterns shows that the nominal composition structures with different concentrations are single phase with no additional lines corresponding to any other phases (except minor traces of CuO in $CuFe_2O_4$ sample as reported [13] previously and shown in Fig. 2).

Tetragonal structure with space group ($I4$) is obtained for $CuFe_2O_4$ and $CuGaFeO_4$ with $c/a > (\sim 1.4)$ as shown in Table 1. This can be explained as the metal

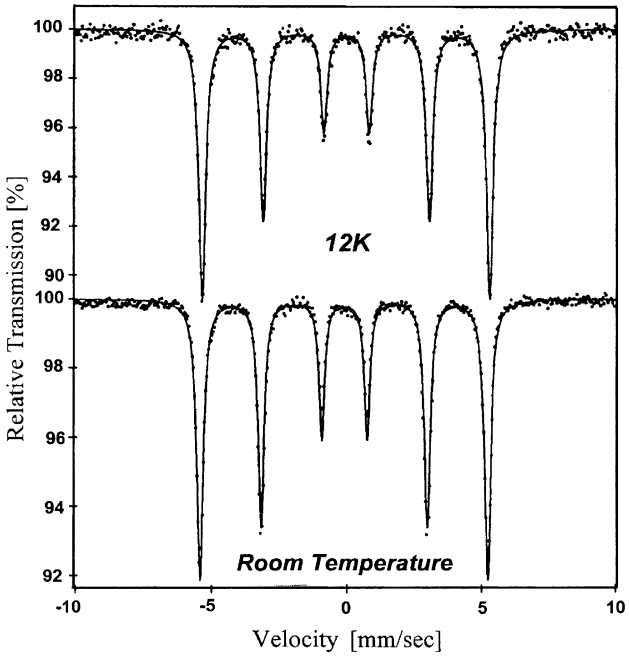

Fig. 1. ME spectra for a pure Fe foil at room temperature and 12 K.

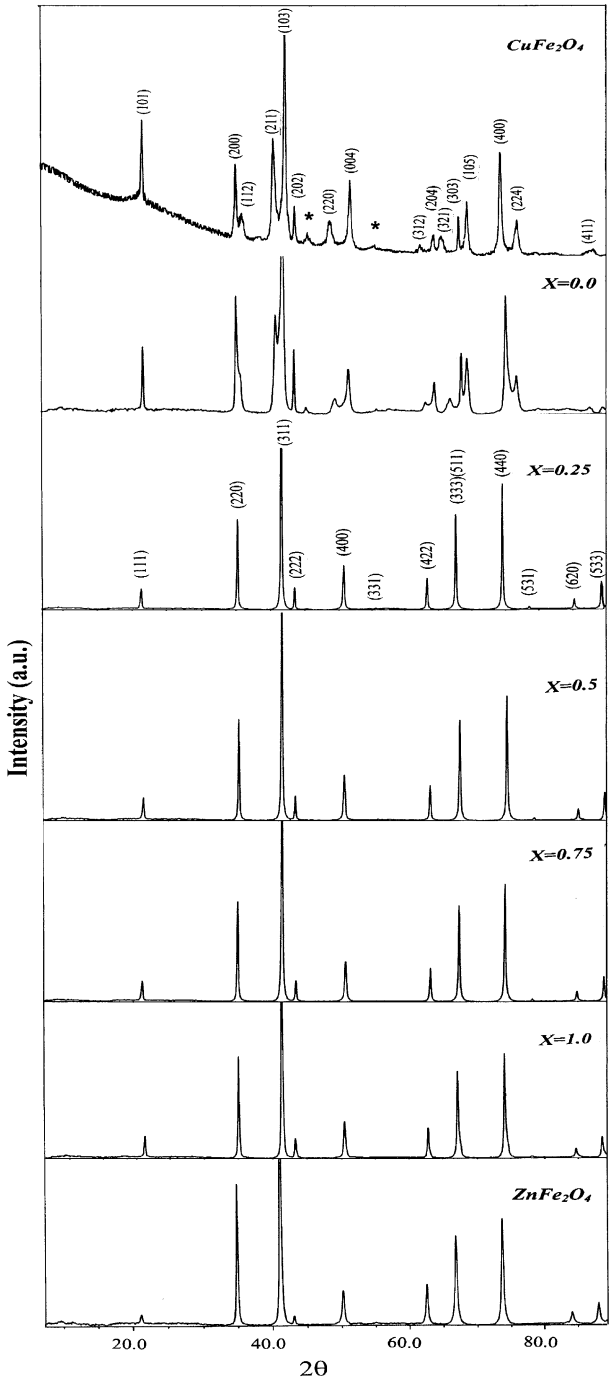

Fig. 2. X-ray powder diffraction patterns at room temperature for $CuFe_2O_4$, $ZnFe_2O_4$ and $Cu_{1-x}Zn_xFeGaO_4$ spinel ferrites (* denotes the CuO traces).

Table 1
Lattice parameters for samples with tetragonal unit cell

Sample	c (Å)	A (Å)	c/a
$CuFe_2O_4$	8.2245(6)	5.9694(8)	1.377
$CuGaFeO_4$	8.2444(2)	5.9416(3)	1.387

sites in most transition metal oxide systems having octahedral site symmetry (D_h), in which each TM ion is surrounded by six oxygen ions, MO_6 as illustrated in Fig. 3. The TM ion becomes tetragonal (D_{4h}) due to the lattice distortion with the elongation of the out-of-phase M–O bonding lengths and the shortening of the in-plane M–O one (as shown in Fig. 3). In more detail, it has been shown that if there is a degenerate orbital state associated with localized d electrons at the TM cation in polar crystal, the structure is unstable to a distortion that provides enough asymmetry to lift the degeneracy. However, a static distortion will occur only if the stabilization energy due to the distortion to lower symmetry is large compared to the separation of the relevant vibrational levels. In a crystal, the magnitude of the stabilization energy depends upon the density of JT ions and the long-range elastic coupling between their interstices as well as on the strength of their interactions with the vibrational modes of the crystal [20]. The cooperative nature of the crystal distortions in these compounds can be rationalized in terms of elastic interactions between the locally distorted polyhedra. Statistical theories of such distortions in spinels (octahedral sites) [21–24] demonstrate that tetragonal structures result from parallel alignments of tetragonally distorted polyhedra in a cubic unit cell.

The tetragonal ($c/a>1.0$) distortions are found at octahedral site Cr^{2+}, Mn^{3+} and Cu^{2+} ions unless the long-range elastic coupling between sites clearly favors another [25]. A distinguishing feature of JT effect found with octahedral site cations having high-spin-state, outer-electron configuration d^4 or d^9 is a strong elastic anisotropy that favors tetragonal ($c/a>1.0$) distortion of the octahedral site (as clearly shown in Fig. 3 for Cu^{2+} and Mn^{3+}). In the available theories of the cooperative JT effect, it is assumed that each polyhedron possesses its own local distortion, ground-state splitting, and stabilization energies, which persist in the

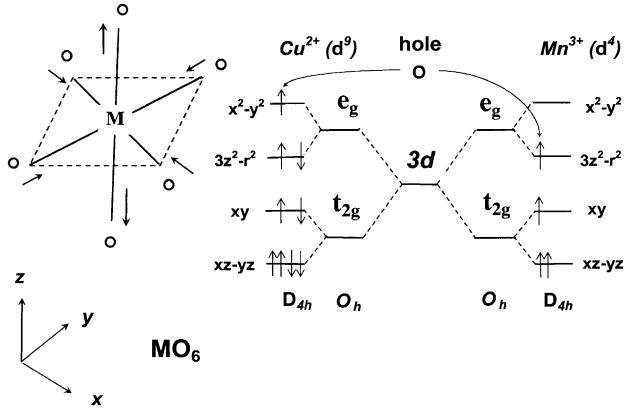

Fig. 3. Tetragonal distortion of MO_6 octahedron and the 3d orbital energy splitting by the octahedron (O_h) and the tetradedral site symmetries for Cu^{2+} (d^9) and Mn^{3+} (d^4) ions under D_{4h} symmetry.

low-symmetry phase. The structural phase transitions appear as a consequence of coupling of local electronic states to bulk deformations and optical phonons of the lattice. The results from optical spectra of many systems [24] demonstrate, that large shifts of the ligand field transitions to higher or lower energies are observed with increasing concentration of the JT ion in host structures with interconnected polyhedron.

In the present study, the tetragonal distortion in $CuFe_2O_4$ and $CuGaFeO_4$ compounds is attributed to the cooperative distortion that is driven by the octahedral Cu^{2+} ($3d^9$) as discussed above. As Zn substitutes for Cu in these distorted spinel ferrites, tetragonal-to-cubic transformation occurs at the compositional parameter ($x \geqslant 0.25$) as shown in Fig. 2. This crystallographic transformation is attributed to the decrease of the concentration of the JT ions [Cu^{2+} ($3d^9$)] in the host structure at the octahedral sites as a result of Zn substitution. This leads to a high-symmetry phase (the cubic phase). The determined lattice parameter a (for samples with cubic unit cell) at different compositional parameter x is given in Table 2 where a increases with increasing Zn content x. This is due to the fact that the Pauling ionic radius of Zn^{2+} (0.74 Å) is greater than that of Cu^{2+} (0.72 Å).

Fig. 4 shows the ME spectrum recorded at 293 K for the stoichiometric $CuFe_2O_4$ sample. This is a well-resolved spectrum consisting of two clearly split Zeeman sextets due to Fe^{3+} at A- and B-sites. In contrast, the ME spectra at 293 K for $Cu_{1-x}Zn_xFeGaO_4$ spinel ferrites in the composition range $0.0 \leqslant x \leqslant 1.0$ and $ZnFe_2O_4$ exhibit quadrupole doublet spectra as illustrated in Fig. 5. The recorded spectra for these samples at 77 K show a relaxed spectra for $x = 0.0$ and 0.25 and quadrupole doublet spectra for compositions with $x \geqslant 0.5$ as shown in Fig. 6. The measured spectra at 12 K for $x = 0.0$, 0.25 and 0.5, show a well-defined absorption lines as seen in Fig. 7. These spectra are fitted with two Zeeman sextets due to Fe^{3+} at the two distinct crystallographic A- and B-sites in the spinel ferrites. Fig. 7 clearly shows a relaxed spectra for samples with $x = 0.75$ and $ZnFe_2O_4$ and quadrupole doublet spectra for $ZnGaFeO_4$ sample.

Table 2
Lattice constant a for $Cu_{1-x}Zn_xGaFeO_4$ samples with cubic unit cell

x	$<a>$ (Å)
0.25	8.3560(7)
0.5	8.3670(9)
0.75	8.3830(8)
1.0	8.3990(7)
$ZnFe_2O_4$	8.4431(9)

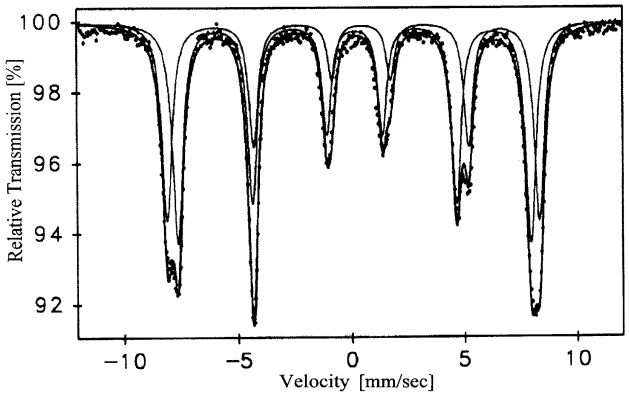

Fig. 4. ME spectra of ^{57}Fe for $CuFe_2O_4$ at 293 and 12 K.

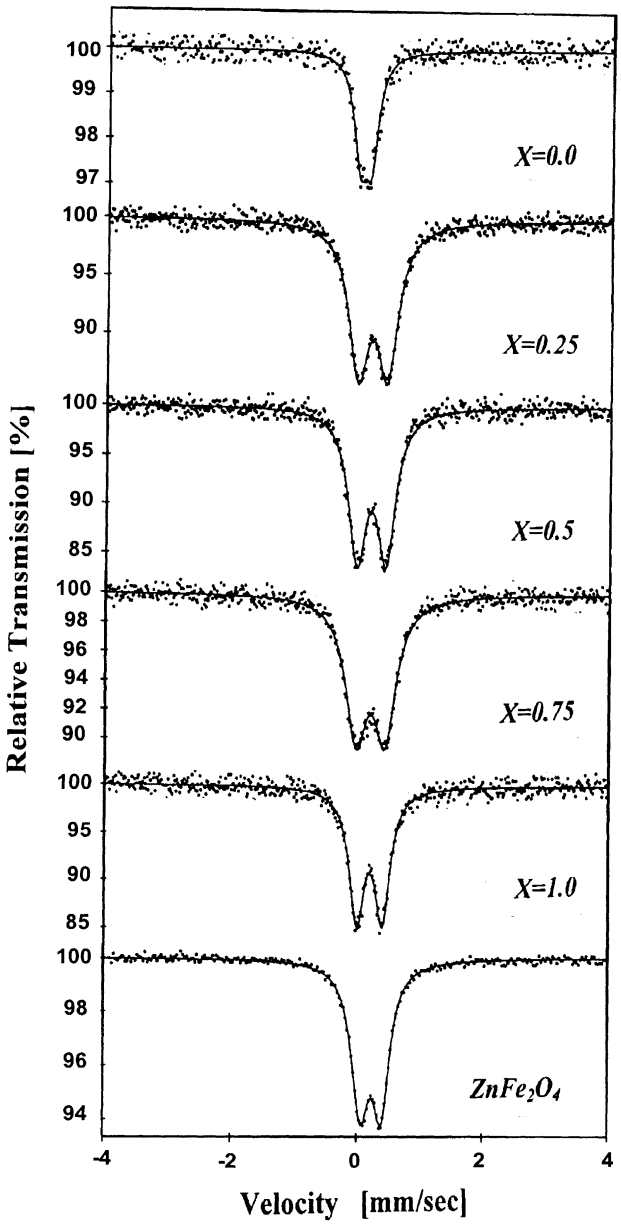

Fig. 5. ME spectra of ^{57}Fe for $ZnFe_2O_4$ and $Cu_{1-x}Zn_xFeGaO_4$ samples at 293 K.

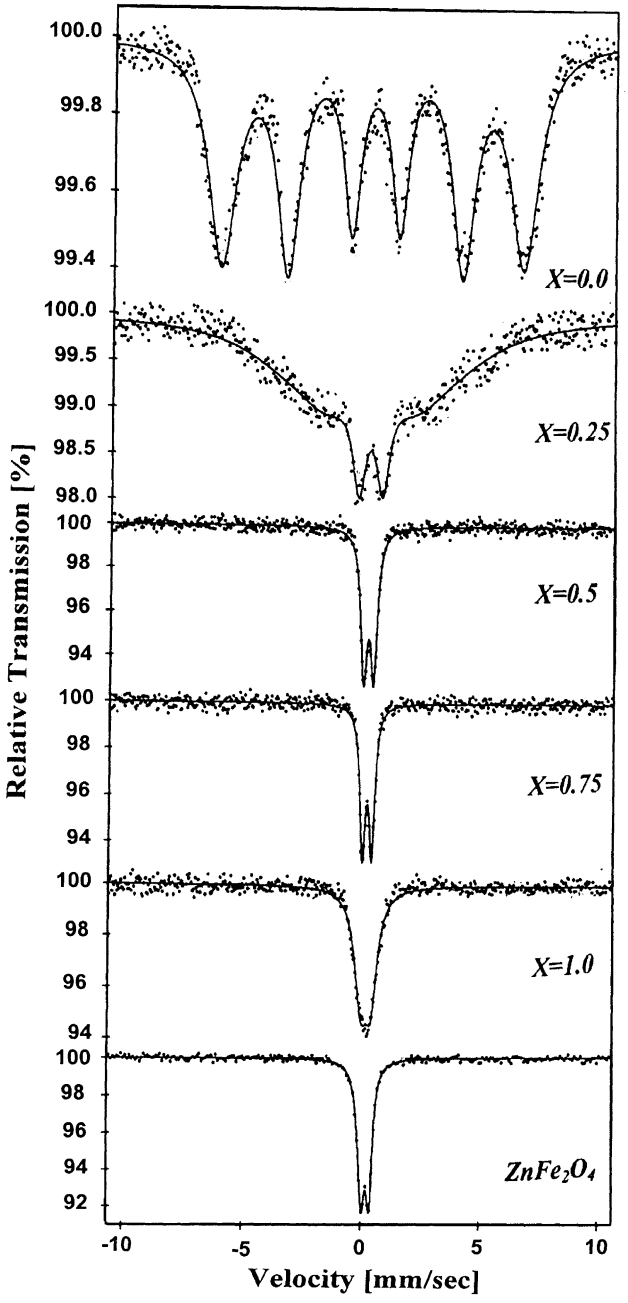

Fig. 6. ME spectra of ^{57}Fe for $ZnFe_2O_4$ and $Cu_{1-x}Zn_xFeGaO_4$ ferrites at 77 K.

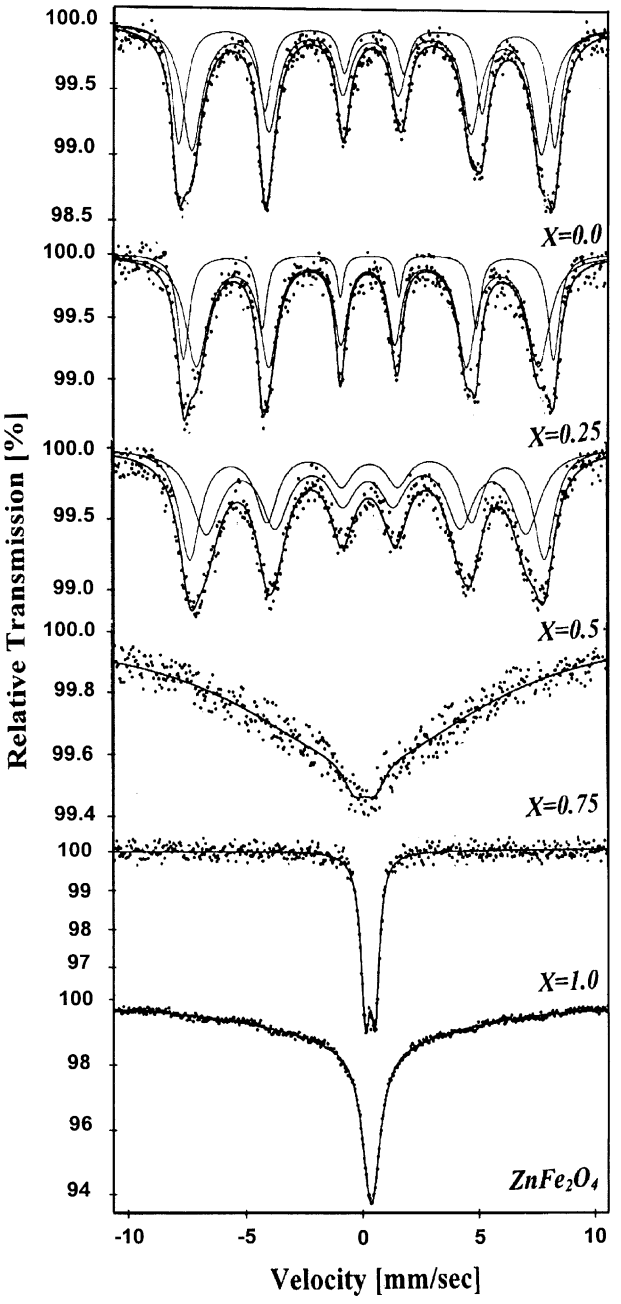

Fig. 7. ME spectra of ^{57}Fe for $ZnFe_2O_4$ and $Cu_{1-x}Zn_xFeGaO_4$ ferrites at 12 K.

The analysis of ME spectra for the compositions under consideration is done using the theories of N magnetic sextets and N quadrupole doublets [18]. In this connection the following points are taken into consideration:

- The magnetic hyperfine splitting contains three pairs of peaks separated with the ratio $\delta_1 : \delta_2 : \delta_3 = 1 : 0.58 : 0.16$, where δ_1 is the relative separation between peaks 1 and 6, δ_2 between 2 and 5 and δ_3 between 3 and 4.
- The hyperfine fields H_{hf} for both A- and B-sites are determined from separation between the centroids of the peaks in each Zeeman pattern.
- Almost, for magnetically ordered spinel ferrites the hyperfine field due to Fe^{3+} at A-sites H_{hfA} is usually smaller than that of Fe^{3+} at B-sites H_{hfB} [27].
- The Zeeman pattern with the smaller isomer shift exhibits the smaller hyperfine field (in agreement with the generally accepted correlation between isomer shifts and hyperfine fields in ferrites) [28].

3.1. Cation distribution

The fraction of iron ions at a distinct crystallographic site can be determined from the ME spectra by knowing the area under the resonance lines due to these ions. In order to get the correct intensity ratio [A/B], the A- and B-site patterns should be well separated. In the simple ferrite $CuFe_2O_4$ sample (Fig. 4), a well-resolved ME spectrum is fitted into two Zeeman sextets with equal areas of A- and B-subspectra. This gives a cation distribution as $(Fe^{3+})[Cu^{2+}Fe^{3+}]O_4^{2-}$ for this simple ferrite, where parenthesis refers to the tetrahedral A-site and square bracket refers to the octahedral B-site. Since, Cu^{2+} ions based on the site-preference energy data [26] and the ME results are occupying the B-site. The resolved spectrum recorded at 12 K (Fig. 7), for $CuFeGaO_4$ sample, is fitted into two sextets due to Fe^{3+} ions at A- and B-sites and gives a cation distribution as $(Fe^{3+}_{0.675}Ga^{3+}_{0.325})[Cu^{2+}Fe^{3+}_{0.325}\ Ga^{3+}_{0.675}]O_4^{2-}$. In addition, the replacement of Cu^{2+} with Zn^{2+} in this spinel ferrite system decreasing the area ratio [A/B] as clearly shown in Table 5. This is due to the occupation of Zn^{2+} at the A-site preferentially, which transfers Fe^{3+} ions to the B-site thus leading to normal spinel at Zn content $x = 1.0$ for $ZnGaFeO_4$ and $ZnFe_2O_4$ samples with cation distributions $(Zn^{2+})[Ga^{3+}Fe^{3+}]O_4^{2-}$ and $(Zn^{2+})[Fe_2^{3+}]O_4^{2-}$, respectively.

3.2. Quadrupole interaction

The presence of chemical disorder in the spinel structure produces an electric field gradient (EFG) of varying magnitude, direction, sign and symmetry and a resulting distribution in the QS. In other words, the EFG at ^{57}Fe nucleus arises from the asymmetrical charge distribution surrounding the ion. However, since an Fe^{3+} ion has a half-filled $3d$ shell ($3d^5$), the EFG in this case can arise only from an asymmetric charge distribution surrounding the iron ion. In a cubic system having Fe^{3+} at both A- and B-sites, the A-site shows a quadrupole splitting due to the asymmetric charge distribution from the 12 B-neighbors. Fe^{3+} ion at B-site has trigonal symmetry and therefore B-sublattice exhibits an EFG with its principal component V_{zz} along the [111] direction. This EFG may arise from departure of the six nearest anion neighbors from their ideal octahedral symmetry and, the non-spherical distribution of charges on the next nearest cation and anion neighbors of the B-site. In the present work, the QS values for the well-ordered spectrum at room temperature for the $CuFe_2O_4$ sample are 0.33 and 0.01 mm s^{-1} for B- and A-sites, respectively. The high value of QS for the B-site clearly demonstrates the presence of chemical disorder due to the tetragonal distortion in this sample as a result of the presence of the JT Cu^{2+} ions at B-site. In addition, the QS values for the tetragonal sample $CuGaFeO_4$ in the well-ordered state at 12 K have the same trend as given in Table 5. However, the QS values for samples with cubic structure ($x \geqslant 0.25$) in the well-ordered state at 12 K are negligible (as seen in Table 5). It could be explained that due to the overall cubic symmetry of the spinel ferrite and randomness of chemical disorder, there will be equal probability for small QSs of opposite signs. Hence, the centers of the Zeeman lines will not change, and consequently there will be no net observable QS. At 293 and 77 K, the QS values of the tetragonal sample $CuFeGaO_4$ are 0.178 and 0.097 mm s^{-1}, respectively, while at 293 K, the QS values for the cubic system $Cu_{1-x}Zn_xFeGaO_4$ with $x \geqslant 0.25$ in the paramagnetic state are in the range of 0.468 and 0.405 mm s^{-1}, which decrease slightly with increasing Zn content x as shown in Table 3. At 77 and 12 K, the values of QS are around $\sim$0.41 mm s^{-1} for these cubic samples in the paramagnetic state (Tables 4 and 5). The values of QS obtained for the $ZnFe_2O_4$ at 293 and 77 K are in good agreement with that reported earlier by Eckert et al. [29].

3.3. Isomer shift

The obtained IS values for $CuFe_2O_4$ sample at 293 K are 0.53 ± 0.01 and 0.41 ± 0.01 mm s^{-1} for the B- and A-sites, respectively, and IS values for $Cu_{1-x}Zn_xFeGaO_4$ spinel ferrites are given in Tables 3–5. The obtained result of IS (A) $<$ IS (B) in the well-ordered spectra is in agreement with other previously reported data [30–32]. This could be interpreted as being due to the large band separation of $Fe^{3+}-O^{2-}$ for the octahedral ions compared with that for the tetrahedral ions. As the orbitals of the Fe^{3+} and O^{2-} ions do not overlap, the covalency effect becomes smaller, and hence the isomer shift is large at the octahedral site. The isomer shifts at 77and 12 K are larger than the values obtained at 293 K due to the second Doppler shift between the source and the absorber at low temperature [33]. There is no significant change of the IS values with Zn content observed in this spinel system. This means that the s electron charge distribution of Fe ions is negligibly influenced by zinc substitution.

Table 3
ME parameters for $ZnFe_2O_4$ and $Cu_{1-x}Zn_xFeGaO_4$ compounds at 293 K

Sample	QS (mm s^{-1})	IS (mm s^{-1})	Line width Γ (mm s^{-1})
$x = 0.0$	0.178 ± 0.009	0.295 ± 0.005	0.261 ± 0.017
$x = 0.25$	0.468 ± 0.003	0.442 ± 0.002	0.395 ± 0.005
$x = 0.5$	0.461 ± 0.003	0.444 ± 0.002	0.351 ± 0.005
$x = 0.75$	0.458 ± 0.004	0.453 ± 0.002	0.421 ± 0.007
$x = 1.0$	0.405 ± 0.003	0.454 ± 0.002	0.297 ± 0.005
$ZnFe_2O_4$	0.333 ± 0.002	0.480 ± 0.001	0.338 ± 0.004

Table 4
ME parameters for$ZnFe_2O_4$ and $Cu_{1-x}Zn_xFeGaO_4$ compounds at 77 K

Sample	H_{hf} (kOe)	QS (mm s^{-1})	IS (mm s^{-1})	Line width Γ (mm s^{-1})
$x = 0.0$	395.4±0.05	0.097±0.010	0.527±0.005	1.418±0.027
$x = 0.25$	195.4±0.55	0.013±0.109	0.443±0.056	—
$x = 0.5$	—	0.419±0.004	0.448±0.002	0.344±0.006
$x = 0.75$	—	0.389±0.004	0.455±0.002	0.290±0.006
$x = 1.0$	—	0.425±0.013	0.452±0.006	0.639±0.022
$ZnFe_2O_4$	—	0.337±0.004	0.457±0.003	0.353±0.011

Table 5
ME parameters for $ZnFe_2O_4$ and $Cu_{1-x}Zn_xGaFeO_4$ compounds at 12 K

Sample	H_{hf} (kOe)		QS [mm s^{-1}]		IS [mm s^{-1}]		Line width Γ [mm s^{-1}]		Area ratio
	B	A	B	A	B	A	B	A	
$x = 0.00$	500.3±0.1	465.4±0.2	0.260±0.013	0.117±0.013	0.588±0.007	0.412±0.007	0.703±0.046	1.02±0.045	0.675
$x = 0.25$	492.6±0.1	455.6±0.2	0.007±0.008	0.011±0.016	0.593±0.008	0.434±0.009	0.706±0.056	1.05±0.068	0.658
$x = 0.50$	471.7±0.2	426.1±0.4	0.076±0.022	0.045±0.026	0.597±0.012	0.437±0.014	0.88±0.0910	1.21±0.128	0.551
$x = 0.75$	166.6±0.3	–	0.053±0.166	–	0.361±0.061	–	–	–	–
$x = 1.00$	–	–	0.415±0.008	–	0.579±0.004	–	0.460±0.012	–	–
$ZnFe_2O_4$	35.7±0.1	–	0.276±0.084	–	0.471±0.042	–	–	–	–

4. Hyperfine fields

The hyperfine magnetic field at the iron nucleus is proportional to the spontaneous magnetization of the sublattice to which the particular nucleus belongs. The hyperfine field H_{hf} measured by the ME consists of three contributions: $H_{hf} = H_{core} + H_{dip} + H_{shift}$, where H_{core} results from the polarization of s electrons by the magnetic moments of the d electrons. This field is larger for free ions than for ions in a crystal because of covalency. H_{dip} represents the dipolar fields produced by the surrounding magnetic ions. This field depends on the distribution of the cation over A- and B-sites. H_{shift} is the supertransferred hyperfine field at a central cation and originate from the magnetic moments of the nearest neighboring cations, i.e., from the intersublattice contributions h_{AA} and h_{BB} and the h_{AB} and h_{BA}. The hyperfine field H_{hf} values for $CuFe_2O_4$ sample at 293 K are 510±0.02 and 484±0.01 kOe for the B- and A-sites, respectively, and at 77 and 12 K for the well-ordered samples of $Cu_{1-x}Zn_xFeGaO_4$ spinel ferrites (with $x =$ 0.0, 0.25 and 0.5) are given in Tables 4 and 5. It can be noticed that the hyperfine field H_{hf} decreases as Zn content x increases. This could be explained as the intersublattice contributions h_{AB} and h_{BA} are predominant at 293 K for the $CuFe_2O_4$ sample. The introduction of Zn^{2+} with closed ($3d^{10}$) shell in the place of Cu^{2+} in this unit cell replaces Fe^{3+} at the tetrahedral A-site and results in the decrease of these intersublattice contributions and in turns decreases the hyperfine field H_{hf} at both sites.

5. Conclusion

The system $Cu_{1-x}Zn_xFe_{2-y}Ga_yO_4$ with ($0.0 \leqslant x \leqslant 1.0$, $y = 0.0$ and 1.0) is successfully prepared with tetragonal unit cell for $CuFe_2O_4$ and $CuGaFeO_4$ due to the presence of JT Cu^{2+} ions at the octahedral site. Tetragonal-to-cubic transformation occurs by replacing Cu^{2+} ion with Zn^{2+} in this system of spinel ferrites. The well-ordered ME spectra are obtained at 12 K after the successful installation and utilization of the closed-cycle variable temperature cryostat for Mössbauer (Model REF-399-D22) where the cation distribution is determined.

References

[1] W.F.J. Fontijn, P.J. van der Zaag, L.F. Feiner, R. Metselaar, M.A.C. Devillers, J. Appl. Phys. 85 (1999) 5100.
[2] A. Zerr, G. Miehe, G. Serghiou, M. Schwarz, E. Kroke, R. Riedel, H. Fuess, P. Kroll, R. Boehler, Nature (London) 400 (1999) 340.
[3] B.N. Kim, K. Hiraga, K. Morita, Y. Sakka, Nature (London) 413 (2001) 288.
[4] A.H. Jahren, M.B. Kruger, R. Jeanloz, J. Appl. Phys. 71 (1992) 1579.
[5] X. Liu, S. Xu, K. Kato, Y. Moritomo, J. Phys. Soc. Japan 71 (2002) 2820.
[6] S. Asbrink, A. Waskowska, J.S. Olsen, L. Gerward, Phys. Rev. B 57 (1998) 4972.
[7] S. Asbrink, A. Waskowska, L. Gerward, J.S. Olsen, E. Talik, Phys. Rev. B 60 (651) (1999) 12.
[8] A. Waskowska, L. Gerward, J.S. Olsen, S. Steenstrup, E. Talik, J. Phys. Condens. Matter 13 (2001) 2549.

[9] P.J. Wojtowicz, Phys. Rev. 116 (1960) 32.
[10] J.D. Duntz, L.E. Orget, J. Phys. Chem. Solids 5 (1957) 20.
[11] R. Enolman, B. Halpertn, Phys. Rev. B 2 (1970) 75.
[12] R. Kanno, N. Kawamoto, Y. Takeda, M. Masegawa, O. Yamamoto, N. Kinomura, J.Solid State Chem. 96 (1992) 397.
[13] X. Tang, A. Manthiram, J.B. Goodenough, J. Solid State Chem. 79 (1989) 250.
[14] A. Navrotsky, O.J. Kleppa, J. Inorg. Nucl. Chem. 29 (1967) 2701.
[15] S.K. Kulshrestha, G. Ritter, J. Mater. Sci. 20 (1985) 821.
[16] A.A. Choni, A.I. Etyhhand, A.A. Mohamed, Proceedings of the International Conference of Ferrites, ICF-5, Japan, 216, 1980.
[17] U. Schwertmann, Adv. Soil Sci. 1 (1985) 171.
[18] S.S. Ata-Allah, M.K. Fayek, H.S. Refai, M.F. Mostafa, J. Solid State Chem. 149 (2000) 434.
[19] M.K. Fayek, S.S. Ata-Allah, H.S. Refai, J. Appl. Phys. 85 (1999) 325.
[20] J.B. Goodenough, J. Phys. Chem. Solids 25 (1964) 151.
[21] P.J. Wojtowicz, Phys. Rev. 116 (1959) 32.
[22] R. Englman, B. Halperin, Phys. Rev. B 2 (1970) 75.
[23] G. Schroder, H. Thomas, Z. Phys. B 25 (1979) 369.
[24] M. Atanasov, U. Kesper, B.L. Ramakrishna, D. Reinen, J. Solid State Chem. 105 (1993) 1.
[25] J.B. Goodenough, in: F.A. Cotton (Ed.), Magnetism and the Chemical Bond, vol. I, Inter-Science, Wiley, New York, 1963.
[26] Xiao-Xio Tang, A. Manthiram, J.B. Goodenough, J. Solid State Chem. 79 (1989) 250.
[27] C.D. Spenser, D. Shroeer, Phys. Rev. B 9 (1974) 3658.
[28] C.A. Sawatzky, F. Vanderwoude, A.H. Morrish, Phys. Rev. 183 (1969) 83.
[29] H. Eckert, C.J. Chen, M. Greenblatt, R.H. Herber, J. Phys. Chem. Solids 49 (1988) 71.
[30] P.R. Edward, C.E. Johnson, R.J.P. Williams, J. Chem. Phys. 47 (1967) 2074.
[31] E. Sionanek, Z. Sroubek, Phys. Rev. 163 (1960) 275.
[32] D.C. Khan, M. Misra, A.R. Das, Phys. Rev. 53 (1982) 2722.
[33] R.V. Pound, G.A. Rebka, Phys. Rev. Lett. 4 (1960) 274.